Macroscopic and microscopic investigation of the antiferromagnetic phase of TbB_6

M. Amara,[1,*] R.-M. Galéra,[1] I. Aviani,[2] and F. Givord[3]
[1]*Institut Néel, CNRS and Université Joseph-Fourier, BP 166X, F-38042 Grenoble, France*
[2]*Institute of Physics, Bijenicka cesta 46, P.O. Box 304, HR-10000 Zagreb, Croatia*
[3]*CEA-Grenoble, INAC/SPSMS/MDN, F-38054 Grenoble, France*
(Received 21 April 2010; revised manuscript received 8 November 2010; published 10 December 2010)

The antiferromagnetic state of TbB_6 has been investigated by means of magnetic susceptibility, magnetostriction, and x-ray diffraction measurements on a single crystal. The anisotropy of the magnetic susceptibility and the magnetostriction data point to a tetragonal symmetry in the antiferromagnetic state. Below T_N, the x-ray diffraction investigation shows the emergence of charge reflections related to wave vectors of the $\langle\frac{1}{2}00\rangle$ and $\langle\frac{1}{2}\frac{1}{2}0\rangle$ types, similar to those observed in GdB_6. The $\langle\frac{1}{2}00\rangle$-type reflections clearly result from the formation of static atomic displacement waves. The stabilization of atomic displacement waves is described as a compromise between the exchange coupling and a single-ion elastic energy. This mechanism is shown to be responsible for the recurrence of the $\langle\frac{1}{4}\frac{1}{4}\frac{1}{2}\rangle$ magnetic wave vectors in rare-earth hexaborides. A combined analysis of experimental and theoretical data points to only two stable tetragonal models for TbB_6 antiferromagnetic structure. This study confirms the influence of exchange displacements in rare-earth hexaborides and highlights the need for a systematic investigation of the magnetic anisotropy of antiferromagnets.

DOI: 10.1103/PhysRevB.82.224411 PACS number(s): 75.10.Dg, 75.25.Dk, 75.30.Et

I. INTRODUCTION

Due to indirect exchange interactions of the Ruderman-Kittel-Kasuya-Yoshida (RKKY) (Ref. 1) type, most rare-earth (RE) intermetallic compounds are magnetically ordered at low temperature. This order is frequently of the antiferromagnetic kind and can take complex forms,[2] well beyond the simple collinear antiphase archetype. This variety of antiferromagnetic (AF) structures is related to the high level of degeneracy that can be expected for the AF state, if only isotropic exchange interactions are taken into consideration. The actual structure then results from a delicate balance between various additional couplings. The first coupling that has to be considered is that of the $4f$ orbitals with the crystal field. The crystal field is the main contributor to the magnetic anisotropy and drastically reduces the AF-state degeneracy. However, for systems with multiaxial symmetry, particularly the cubic one, taking into account the crystal field and bilinear exchange interactions does not point to a unique antiferromagnetic model. In particular, to explain the energy difference between a collinear and a multiaxial magnetic structure, additional pair interaction terms are needed. For this purpose, an orbital mechanism is usually invoked, namely the quadrupolar couplings between the $4f$ ions or between the ions and a lattice striction mode (i.e., the magnetoelastic coupling). These orbital couplings have been shown to determine not only the multiaxial nature of the magnetic structures but also to induce sizable magnetostriction phenomena and, as well as the crystal field, to influence the magnetic transitions in their type (first or second order), critical field and temperature.[3] They are thus central in the understanding of the features of the antiferromagnetic range of cubic $4f$ systems. However, they cannot be invoked when complex antiferromagnetic properties are observed in systems where the $4f$ ions lack an orbital degeneracy. In the case of GdB_6, it has been established that the exchange driven displacements of the Gd ions are responsible for the peculiarities of the antiferromagnetic order:[4,5] the first-order magnetic transition at T_N and the succession in temperature of two spontaneous AF phases, that would have been otherwise ascribed to orbital effects. The signature of this alternative mechanism is the development, below T_N, of static atomic displacement waves that were characterized using single crystal x-ray diffraction.[5,6]

In principle, the influence of the exchange displacements should not restrict to $L_{4f}=0$ compounds and can be considered for any system with a favorable crystallographic structure. This is the case of the rare-earth hexaboride series, where the CaB_6-type structure (space group $Pm\bar{3}m$) leaves some latitude of movement for the rare-earth ion inside its boron cage. To check the relevance of the exchange displacement mechanism for other elements within this series, we have turned our attention to the TbB_6 compound. Extrapolated according to the de Gennes law, the effects of the displacements in TbB_6 should be comparable to those in GdB_6. In this regard, one can expect a first-order transition at T_N, without need of invoking a crystal-field effect.

There are indeed experimental indications, via specific heat,[7] magnetic,[8] elastic[9] measurements, and powder neutron diffraction,[10] of a first-order magnetic transition in TbB_6 at $T_N=19.5$ K (this temperature seems to be strongly sample dependent, the values in the literature[8,11] ranging from 17.4 to 21 K). The powder neutron-diffraction patterns can be indexed considering $\langle\frac{1}{4}\frac{1}{4}\frac{1}{2}\rangle$ magnetic wave vectors,[10] as in GdB_6, but, unlike this latter, a single AF phase is stable down to the lowest temperatures in TbB_6. Due to the intrinsic ambiguities[13] of powder neutron diffraction, the actual magnetic structure cannot be derived from these experiments. It could be determined from additional neutron scattering experiments on a single crystal, under an applied magnetic field, but this would require the preparation of a specific sample using ^{11}B enriched boron. As good quality single crystals, although not ^{11}B enriched and, alternative, macroscopic and microscopic, experimental techniques were avail-

able, we undertook a extensive investigation of TbB_6 AF state without resorting to single crystal neutron diffraction.

In this paper, we thus present a study of TbB_6 antiferromagnetic state which combines macroscopic (magnetic susceptibility, magnetostriction) and microscopic (x-ray diffraction) techniques applied to a single crystal. The anisotropy of the antiferromagnetic susceptibility is characteristic of the macroscopic symmetry and, once determined, is a mean for controlling the sample's domain distribution. Thereafter, the magnetostriction measurements can provide a quantitative characterization of the antiferromagnetic symmetry lowering. In rare-earth compounds, the magnetostriction phenomena mainly reflects the $4f$ shell distribution changes at the zone center. Outside the zone center, x-ray diffraction is well suited for revealing charge arrangements associated with the antiferromagnetic state (atomic displacements or multipolar arrangements).

The experimental part of this paper divides into three sections. The first section is devoted to the antiferromagnetic susceptibility measurements and their analysis based on domains selection. The second section deals with the magnetostriction measurements and, again, with the delicate point of domains effects. In the last experimental section, the x-ray scattering experiments, aimed at the detection of reflections specific to the AF state, are presented. In the second part of the paper, a joint analysis of the different experimental and theoretical data is carried out in order to define consistent models for TbB_6 magnetic structure. The physical relevance of these structures is checked using a mean-field model which accounts for the exchange displacements phenomena.

II. EXPERIMENTAL PART

Considering a crystallographic system with a single magnetic ion per cell, the transition from the paramagnetic to the antiferromagnetic state is characterized by the loss of part of the translation group elements (the antiferromagnetic cell is bigger than the paramagnetic one) and part of the rotation group (due to the orientation of the magnetic moment along a single or a few particular axes of the crystal). To detect changes in the translational symmetries a microscopic probe is needed. Since decades, neutron diffraction has been the most effective tool for magnetic structure determination. The alternative x-ray probe is weakly sensitive to magnetism but is optimal for detecting new charge periodicities in relation with the magnetic order.

The loss of point symmetries at the antiferromagnetic transition can be tracked via macroscopic experimental techniques. Indeed, according to Neumann's principle, the anisotropy of a crystal tensorial property is dictated by the point symmetries of the magnetic cell. The careful investigation of a physical property should yield valuable data, not only in terms of a physical quantitative determination but also as a probe of the system symmetry in the AF state.

A. Macroscopic investigation

With the loss of symmetry below T_N, a single crystal inevitably divides into areas, the domains, which, despite a common point group, differ in their singular elements of symmetry.[29] Without the knowledge of these domain distribution, bulk measurements on the crystal yield an extrinsic average. Thus the determination of any anisotropic physical property is strongly hampered. In the following, regardless of spatial continuity, we consider that all the parts of the sample sharing the same point symmetry elements belong to the same domain. In the academic case of domains equipartition, the macroscopic average should restore, in appearance, the symmetry of the paramagnetic state. To reveal the hidden anisotropy, one has to establish a well-defined unbalanced domain distribution. This can be achieved by submitting the sample to some anisotropic field. In magnetic systems, the most obvious candidate is a magnetic field. In principle, for a given field direction, due to the different magnetic susceptibilities, the chemical potentials of the various domains will develop differently with the field amplitude. Accordingly the domain walls will move until the sample reaches a single-domain state (in a less ideal case, a degeneracy can persist between domains of equivalent symmetry). This state will allow an accurate determination of all the sought anisotropic properties, but to achieve this it requires the prior knowledge of the magnetic-susceptibility anisotropy. Thus the investigation of any macroscopic, possibly anisotropic, property should begin with a careful determination of the antiferromagnetic susceptibility. In the following section, this question is addressed by a systematic consideration of the various situations of symmetry lowering, then of anisotropy of the magnetic susceptibility. This methodology is applied to the investigation of the AF-state magnetic susceptibility in TbB_6, in order to subsequently determine another tensorial property characteristic of the AF state: the spontaneous magnetostriction.

The sample used in all the experiments is a single crystalline sphere of 3.5 mm diameter. The crystal growth methods are detailed in Ref. 12.

1. Magnetic susceptibility

a. Methodology. The static magnetic susceptibility is a real symmetric tensor of rank 2, which means that, along the principal axes of the system, it can be written as a 3×3 diagonal matrix with up to three distinct elements. This number of elements reduces to one in the highly symmetric case of cubic systems in the paramagnetic state, the only systems we shall here consider.[13] Below the Néel point, the symmetry of the crystal may change in accordance with the new point symmetries of the magnetic arrangement. AF states that keep the cubic symmetry of the paramagnetic state are not uncommon in systems with multiaxial antiferromagnetism as, for instance, DyCu,[14] $TmGa_3$,[15] or NdZn.[16] In such cases the magnetic susceptibility remains isotropic as well as all the bulk physical quantities. In AF states with point symmetry lower than cubic, the induced anisotropy leads to an increase in the number of independent elements in the susceptibility tensor. Two different values on the diagonal is the first degree to consider for describing this emerging anisotropy. This happens for a system with a single n-fold axis with n higher than two: starting from a cubic symmetry, the relevant situations are those of tetragonal or trigonal symmetry lowering

TABLE I. Effective magnetic susceptibilities χ_{xyz} of a cubic crystal undergoing a tetragonal or trigonal symmetry lowering, for a magnetic field applied along $[xyz]$. They are obtained from the list of the field selected domains (between {}) as expected from the hierarchy between the two normal susceptibilities $\chi_{\parallel}$ and $\chi_{\perp}$, respectively, parallel and perpendicular to the fourfold or threefold axis (see text). The characteristic inequalities and equations, between the effective susceptibilities, are, respectively, given in the lines entitled Sequ. and Equ.

	Tetragonal				Trigonal			
	$\chi_{\parallel}>\chi_{\perp}$		$\chi_{\perp}>\chi_{\parallel}$		$\chi_{\parallel}>\chi_{\perp}$		$\chi_{\perp}>\chi_{\parallel}$	
$[xyz]$	Domains	χ_{xyz}	Domains	χ_{xyz}	Domains	χ_{xyz}	Domains	χ_{xyz}
[001]	{001}	$\chi_{\parallel}$	{100,010}	$\chi_{\perp}$	$\{111,11\bar{1},1\bar{1}1,\bar{1}11\}$	$\frac{1}{3}(\chi_{\parallel}+2\chi_{\perp})$	$\{111,11\bar{1},1\bar{1}1,\bar{1}11\}$	$\frac{1}{3}(\chi_{\parallel}+2\chi_{\perp})$
[110]	{100,010}	$\frac{1}{2}(\chi_{\parallel}+\chi_{\perp})$	{001}	$\chi_{\perp}$	$\{111,11\bar{1}\}$	$\frac{1}{3}(2\chi_{\parallel}+\chi_{\perp})$	$\{1\bar{1}1,\bar{1}11\}$	$\chi_{\perp}$
[111]	{100,010,001}	$\frac{1}{3}(\chi_{\parallel}+2\chi_{\perp})$	{100,010,001}	$\frac{1}{3}(\chi_{\parallel}+2\chi_{\perp})$	{111}	$\chi_{\parallel}$	$\{11\bar{1},1\bar{1}1,\bar{1}11\}$	$\frac{1}{9}(\chi_{\parallel}+8\chi_{\perp})$
Sequ.	$\chi_{001}>\chi_{110}>\chi_{111}$		$\chi_{110}=\chi_{001}>\chi_{111}$		$\chi_{111}>\chi_{110}>\chi_{001}$		$\chi_{110}>\chi_{111}>\chi_{001}$	
Equ.	$\chi_{110}=\frac{3}{4}\chi_{111}+\frac{1}{4}\chi_{001}$		$\chi_{110}=\chi_{001}$		$\chi_{110}=\frac{1}{2}\chi_{111}+\frac{1}{2}\chi_{001}$		$\chi_{110}=\frac{3}{2}\chi_{111}-\frac{1}{2}\chi_{001}$	
$\chi_{\parallel}$	χ_{001}		$2\chi_{001}-\chi_{110}$		χ_{111}		$\chi_{001}-2\chi_{110}$	
$\chi_{\perp}$	$\frac{1}{2}(3\chi_{111}-\chi_{001})$		χ_{110},χ_{001}		$\frac{1}{2}(3\chi_{001}-\chi_{111})$		χ_{110}	

where, respectively, a fourfold or threefold rotation axis is preserved. If the symmetry is further reduced, the crystal symmetry belongs to the orthorhombic, triclinic, or monoclinic systems, in which cases three distinct values are needed to describe the system susceptibility. However, such drastic symmetry reductions are less likely in cubic rare-earth compounds[3] and the analysis is here restricted to the tetragonal and trigonal cases.

The tetragonal and trigonal crystal systems have two characteristic values for the susceptibility that we denote by $\chi_{\parallel}$ and $\chi_{\perp}$ for field directions, respectively, parallel and perpendicular to the fourfold and threefold axis. The analysis of the field selection of domains is based on the contrast between these two susceptibilities. The first step is to establish the list of the domains that coexist in the AF state. For the tetragonal case, three domains are expected which differ in their respective fourfold axes, parallel to the three fourfold directions of the cubic paramagnetic phase. Similarly, there are four trigonal domains, each one having its threefold axis along one of the paramagnetic cubic threefold axis. Once the domains are listed, according to the hierarchy between $\chi_{\parallel}$ and $\chi_{\perp}$, one can predict which domains will be selected for a given field direction: i.e., the domains whose "easy" antiferromagnetic axis is the closest to the field direction (this approach is analog to Néel's "phases rule" for ferromagnets[17]). After completion of the field selection, the sample state is perfectly defined as regards the domains distribution. At this stage, any anisotropic property can be, in principle, accurately determined using the appropriate experimental means. Tables I summarizes the effect of the domains selection, within the tetragonal or trigonal hypothesis, for a magnetic field applied along the cube's high-symmetry directions and according to the hierarchy between $\chi_{\parallel}$ and $\chi_{\perp}$. The selected domains are listed between braces {} with indices referring to the direction of their fourfold or threefold axis. As a result of the analysis, the effective susceptibility χ_{xyz}, for a field applied along $[xyz]$, is defined as a linear combination of $\chi_{\parallel}$ and $\chi_{\perp}$. Characteristic inequalities and equations between the effective susceptibilities are thus obtained which should allow the identification of both the symmetry lowering (tetragonal or trigonal) and inequality between $\chi_{\parallel}$ and $\chi_{\perp}$.

Conversely, this analysis allows the determination of $\chi_{\parallel}$ and $\chi_{\perp}$ from susceptibility measurements along the crystal high-symmetry directions (see the definitions on the last two lines of Table I).

b. Measurements. Magnetization measurement were performed at the Institut Néel. The used setup is an extraction-type magnetometer, with a sensitivity better than 10^{-5} emu and an accuracy of about 0.1%. The available field range goes up to 10.5 T, while the sample can be cooled from 300 K down to 1.5 K in a helium flux cryostat. Two kinds of measurements were performed:

(i) Constant temperature, with a field excursion from 0 to 8 T, then from 8 to 0 T. The susceptibility was then derived using the Arrott method[18] restricted to the decreasing field part of the measurements. In this way, the data comes from a sample where the domains distribution has been imposed by the applied field.

(ii) Constant field $\mu_0 H=1$ T, for a temperature increasing from $T=2.5$ K up to 30 K. Prior to this temperature variation, the field was swept from 0 to 8 T, then down to 1 T in order to ensure proper domains selection. It is assumed that the domain partition is then stable up to T_N.

Figure 1 shows the magnetization loops measured along the three main directions of the cube at $T=3$ K, for a field sweep 0–8-0 T. The fourfold axis is the only direction for which a clear hysteresis is observed, i.e., an irreversible change in the domains distribution. The initial susceptibility is very similar for the three field directions, which is indicative of near equipartition of the domains for the sample virgin state. The apparent isotropy disappears at 5.5 T, as the fourfold axis curve displays a sudden upward jump. There is no reverse effect as the field is decreased, the sample having reached a new, apparently stable, domains distribution. This is in contrast with the threefold axis situation, for which the magnetization in increasing or decreasing the field is almost superimposable. Except for a sudden increase of the curve slope above 7 T, which is due to the proximity of a field induced phase transition,[8] the measurements along the twofold direction show no accident and very little hysteresis.

These low temperature measurements show that TbB_6 AF-state susceptibility is anisotropic, with a clear "easy axis"

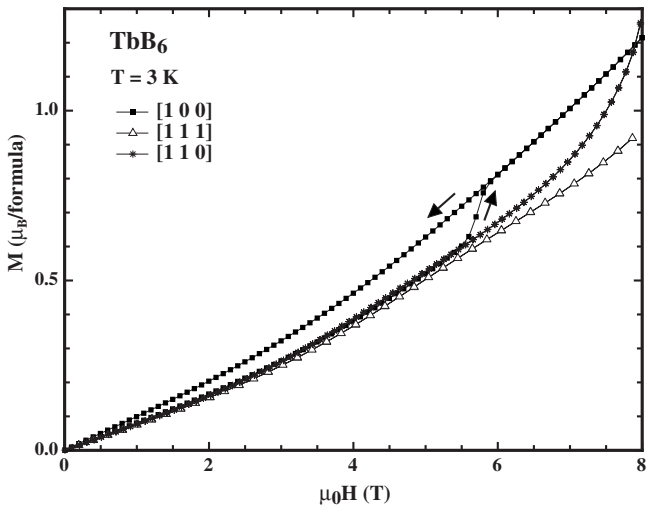

FIG. 1. Magnetization loops at $T=3$ K measured along three high-symmetry axes of a TbB_6 single crystal.

character for the [100] direction. Less contrast is observed between the [110] and [111] directions. However, if one considers more carefully the curves for decreasing fields close to zero, the magnetization appears to be slightly larger along the twofold axis than along the threefold one.

From the Arrott determinations of the susceptibilities, this hierarchy, $\chi_{001} > \chi_{110} > \chi_{111}$, generalizes to the whole antiferromagnetic range of TbB_6 (Fig. 2). As expected from the weakening of the anisotropy while increasing the temperature, the advantage of the fourfold axis over the twofold and threefold axis decreases as T_N is approached. At T_N, the first-order character of the transition from the antiferromagnetic to the paramagnetic state is evident in the upward jump of the susceptibility. The magnetization measurements under a constant field $\mu_0 H=1$ T (connected dots on Fig. 2), provide a faithful approximation of the Arrott determination. They

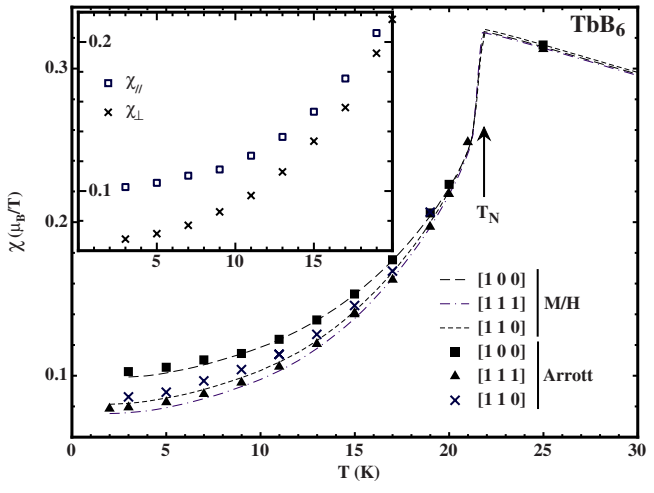

FIG. 2. (Color online) Magnetic susceptibilities of a TbB_6 single crystal along the three high-symmetry directions. The large full dots results from the Arrott method, whereas the lines represent the ratio $M/\mu_0 H$ for $\mu_0 H=1$ T. The inset gives the thermal dependence of the normal susceptibilities, $\chi_{\parallel}$ and $\chi_{\perp}$, as deduced from the relations in Table I.

show no discontinuity while heating the sample up to T_N, which attests to the stability of the domains distribution obtained after the initial field sweep. The slight difference with the Arrott determination results from higher orders susceptibilities which already interfere under a 1 T applied field.

As discussed in the methodology section, Table I, the dominant fourfold susceptibility, with minimal susceptibility along the threefold direction, is characteristic of a tetragonal symmetry with maximum susceptibility along the fourfold axis. This can be checked up to a quantitative level using the equation $\chi_{110}=\frac{3}{4}\chi_{111}+\frac{1}{4}\chi_{001}$ from Table I. The χ_{110} value thus deduced from χ_{111} and χ_{001} compares very well with the direct experimental determination. From the relations in Table I, the two tetragonal susceptibilities, $\chi_{\parallel}$ and $\chi_{\perp}$, can be derived from the measurements and their thermal dependence is reported in the inset of Fig. 2.

Beyond this phenomenological analysis, the anisotropy of the antiferromagnetic susceptibility gives some indication regarding the magnetic structure of TbB_6. In order to get a higher susceptibility along the fourfold axis, the magnetic moments most likely lie perpendicular to this same axis. The fourfold symmetry implies that, within the plane perpendicular to the fourfold axis, there are at least two distinct directions for the magnetic moments: the magnetic structure of TbB_6 is thus necessarily multiaxial.

2. Magnetostriction

a. Methodology The framework used to analyze the magnetostriction data is that of the cubic normal strain modes[19] $(\epsilon^{\alpha}, \epsilon_1^{\gamma}, \epsilon_2^{\gamma}, \epsilon_1^{\epsilon}, \epsilon_2^{\epsilon}, \epsilon_3^{\epsilon})$. In that context, using the definitions of Ref. 3 and along an axis of direction cosines $(\beta_x, \beta_y, \beta_z)$, the sample elongation $\lambda=\frac{dl}{l}$ is related to the normal strain modes via the equation:

$$\lambda_{\beta_x\beta_y\beta_z} = \frac{1}{\sqrt{3}}\epsilon^{\alpha} + \frac{1}{\sqrt{6}}[(3\beta_z^2-1)\epsilon_1^{\gamma} + \sqrt{3}(\beta_x^2-\beta_y^2)\epsilon_2^{\gamma}] + \sqrt{2}[\beta_x\beta_y\epsilon_1^{\epsilon} + \beta_y\beta_z\epsilon_2^{\epsilon} + \beta_z\beta_x\epsilon_3^{\epsilon}]. \quad (1)$$

In the present case of a phase transition with a symmetry lowering from cubic to tetragonal, choosing the z axis as the fourfold axis, only two normal modes will contribute to the sample elongation: $\epsilon_1^{\gamma}=\epsilon^{\gamma}$ and ϵ^{α}, respectively, describing the tetragonal and the volume strain modes. In this context, Eq. (1) reduces to

$$\lambda_{\beta_x\beta_y\beta_z} = \frac{1}{\sqrt{3}}\epsilon^{\alpha} + \frac{1}{\sqrt{6}}(3\beta_z^2-1)\epsilon^{\gamma}. \quad (2)$$

The volume mode ϵ^{α} is needed to account for both the usual thermal expansion and the specific volume magnetostriction that should be present, even if small. Determining the two quantities, ϵ^{γ} and ϵ^{α}, requires at least two experimental configurations for the measurement of the sample elongation. In order to rigorously define these configurations, one has to consider the results of the antiferromagnetic susceptibility investigation: the symmetry lowering being identified as tetragonal and the maximum susceptibility as $\chi_{\parallel}$, the sample direction which should be sensed, as well as the optimal field directions for domains selection can be defined.

TABLE II. Domains selection, according to the magnetic field direction, and deduced elongation along the [001] crystal direction in case of a tetragonal symmetry lowering with maximum magnetic susceptibility along the preserved fourfold axis. The selected domains are named after the indices of their respective fourfold axis. The star (*) indicates that equipartition is assumed for defining the sample's elongation.

Field direction	Selected domains	$\lambda//[001]$
[001]	{001}	$\frac{1}{\sqrt{3}}\epsilon^{\alpha}+\frac{2}{\sqrt{6}}\epsilon^{\gamma}$
[100]	{100}	$\frac{1}{\sqrt{3}}\epsilon^{\alpha}-\frac{1}{\sqrt{6}}\epsilon^{\gamma}$
[110]	{100,010}	$\frac{1}{\sqrt{3}}\epsilon^{\alpha}-\frac{1}{\sqrt{6}}\epsilon^{\gamma}$
[011]	{010,001}*	$\frac{1}{\sqrt{3}}\epsilon^{\alpha}+\frac{1}{\sqrt{6}}\epsilon^{\gamma}$
[111]	{100,010,001}*	$\frac{1}{\sqrt{3}}\epsilon^{\alpha}$

According to Eq. (1), for a tetragonal symmetry lowering, the maximum elongation/contraction of the sample develops along the [100], [010], or [001] directions. The optimal direction along which to probe the sample's changes in length is then a fourfold axis of the initially cubic crystal. In our experiments, this axis of elongation is referred to as [001]. The observed changes in length will depend on the domains distribution, thus on the direction of the applied magnetic field. The expected domains distributions and sample elongations along [001] for relevant high-symmetry directions of the applied field are listed in Table II. In case the selected domain is not unique, the reported sample elongation is derived by linearly composing the contributions of the present domains with, if necessary (indicated by the symbol "*" in Table II), the additional hypothesis of equipartition.

From Table II, it appears that the most reliable determinations of the sample elongation along [001] are obtained for a magnetic field directed along [001], [100], and [110]. For the H//[001] and H//[100] configurations, the sample reaches a single domain state, whereas for H//[110], the two selected domains equally contribute to the elongation. The configuration with parallel magnetic field and measured elongation yields $\lambda_{//}=\frac{1}{\sqrt{3}}\epsilon^{\alpha}+\frac{2}{\sqrt{6}}\epsilon^{\gamma}$, parallel to the fourfold axis of the single domain. The other two configurations result in the elongation perpendicular to the fourfold axis of the tetragonal AF structure: $\lambda_{\perp}=\frac{1}{\sqrt{3}}\epsilon^{\alpha}-\frac{1}{\sqrt{6}}\epsilon^{\gamma}$. Combining these two elongations yields the sought normal strain modes as

$$\epsilon^{\alpha}=\frac{1}{\sqrt{3}}(\lambda_{//}+2\lambda_{\perp}),$$

$$\epsilon^{\gamma}=\epsilon_1^{\gamma}=\sqrt{\frac{2}{3}}(\lambda_{//}-\lambda_{\perp}). \quad (3)$$

b. Experiments The spontaneous magnetostriction in the antiferromagnetic state of TbB_6 has been investigated using the magnetostriction apparatus of the "Institut Néel." This setup uses the capacitance method for dilatometric measurements in the temperature range 2.5–300 K and in magnetic fields up to 6.5 T. The CuBe capacitance cell, which is sensitive to sample length changes along a horizontal direction, can be rotated around the vertical axis of the cryostat. As the magnetic field, provided by a superconducting split-coil, is also horizontal, it is possible to adjust, from 0 to 360°, the angle θ between the probed axis of the sample and the field direction. Typical resolution is about 1 Å, which, for usual millimetric sample dimensions, represents a sensitivity better than 10^{-7}. The spherical sample was glued so as to have two fourfold axes, [100] and [001], within the horizontal plane, the elongation being measured along [001] axis (see inset of Fig. 3). With a single gluing of the sample, this geometry gives access to the configurations listed in the first two lines of Table II. This means that, provided domain selection is achieved, $\lambda_{//}$ can be measured for $\theta=0°$, whereas $\theta=90°$ yields $\lambda_{\perp}$.

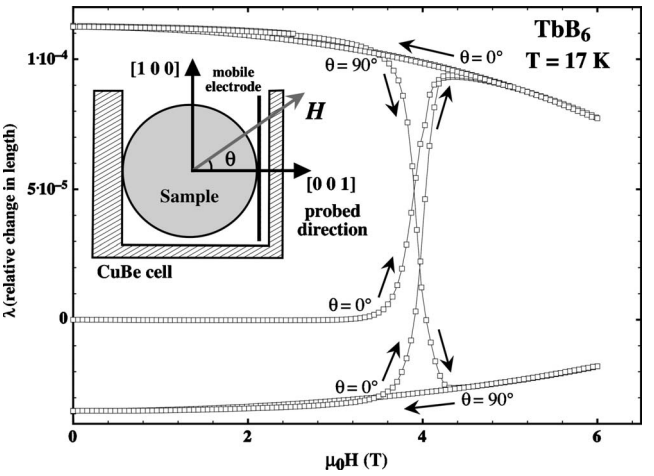

FIG. 3. Loops of relative elongation of a TbB_6 single crystal along the [001] direction showing the two single domain states accessible for the chosen sample configuration (as schematized in the inset which represents the capacitance cell of the dilatometer). The sample is initially virgin with reference length taken at $H=0$ and $\theta=0°$. The field direction is successively rotated in zero field in the sequence $0°-90°-0°$.

Cooling down the sample under zero magnetic field does reveal a small anomaly in the sample length as T_N is crossed. The amplitude of this anomaly is minute in comparison with what develops as the magnetic field is increased for $\theta=0°$ below T_N. Figure 3 illustrates the drastic changes in length that occur at $T=17$ K, starting from a virgin state of the sample and successively applying the magnetic field along [001] ($\theta=0°$) and [100] ($\theta=90°$). Between 3.5 and 4 T, a step of relative amplitude larger than 10^{-4} is observed. In the first field sweep, for $\theta=0°$, one observes that after the upward jump, no further anomaly can be detected while increasing or decreasing the field. The sample has evidently reached a stable domains distribution. To destabilize this distribution, the field has to be applied along another direction; proceeding with a field direction along [100] ($\theta=90°$), a downward jump in the relative elongation is obtained at the same field amplitude, close to 3.8 T. The sample state that is reached in that way is also stable with respect to any further field variation. For both stable domains distributions, the only field effect is a smooth quadratic evolution. This can be interpreted as the forced magnetostriction that accompanies the progressive field distortion of the antiferromagnetic structure. This observed stability of the domain distribution

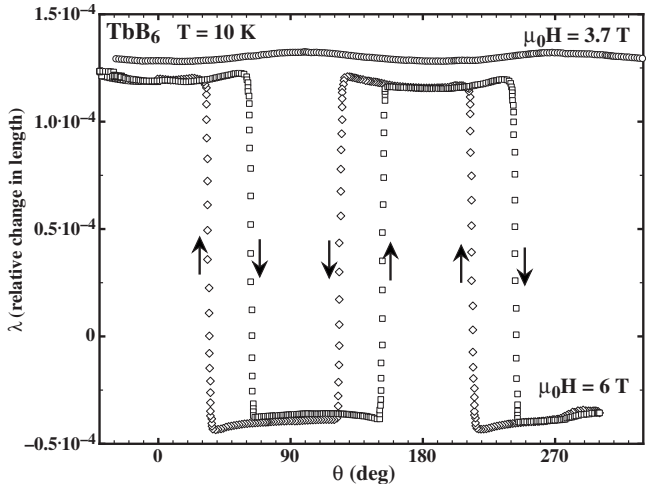

FIG. 4. Lower curve: relative elongation, for a constant field $\mu_0 H=6$ T and variable field angle θ, showing the hysterical domain-switching of the TbB_6 single crystal. Upper curve: equivalent measurements for $\mu_0 H=3.7$ T.

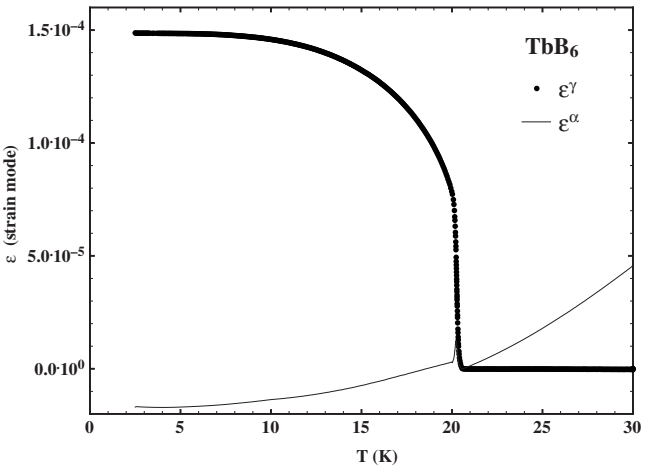

FIG. 5. The two normal strain modes of TbB_6: ϵ^{γ} (tetragonal, black dots) and ϵ^{α} (volume, full line) as measured taking advantage of the single domain states of the single crystal.

is consistent with the single domain character expected from the analysis of the magnetic susceptibility: applying the field along a fourfold direction of the initially cubic crystal results in the selection of a single tetragonal domain below T_N.

Measuring the sample length, as a function of the angle θ for constant field and temperature, provides even more spectacular evidence for the switching between two single domain states of the sample. As shown in Fig. 4, for low field amplitudes ($\mu_0 H=3.7$ T), the only effect is a slight undulation of the sample length, while for a high enough amplitude ($\mu_0 H=6$ T), the sample periodically switches between the two states. There is some delay in the switching which results in the observed hysteretical behavior, but the critical angles are about 45°, 135°, and 225°, exactly at midpoints between the two fourfold directions in the plane. From the analysis of the antiferromagnetic susceptibility, the single domain obtained for $\theta=0°$ (or $\theta=180°$) has its fourfold axis and maximum susceptibility along the probed sample length. For $\theta=90°$ (or $\theta=270°$), the probed sample length is perpendicular to the single domain fourfold axis. Consequently, during the rotation, $\lambda_{//}$ and $\lambda_{\perp}$ are the successive elongations that the capacitance cell detects, with a 180° period.

The observed stability of the single domain state is particularly valuable in the quantitative determination of the tetragonal striction mode. Indeed, once the single domain state is reached, the field can be removed and the subsequent measurement of the temperature dependent elongation, $\lambda_{//}(T)$ or $\lambda_{\perp}(T)$, reflects the spontaneous magnetostriction (in addition to the normal thermal expansion). Despite the absence of a demagnetizing field effect and its *a priori* minimal elastic energy, a single domain state in zero magnetic field is rather uncommon. In most cases, internal stresses or other defects will help restoring the minority domains as the field is decreased; to maintain the single domain state requires the constant application of a magnetic field of non-negligible amplitude. In those circumstances, the measured elongation includes a forced magnetostriction in addition to the spontaneous phenomena (see, for instance, the case of NdMg in Ref. 20). This unusual stability of the single domain state is a feature of TbB_6 and/or a testimony to the quality of the used single crystal.

Figure 5 shows the temperature dependence of the two strain modes, as deduced, using Eq. (3), from the measurement of $\lambda_{//}(T)$ and $\lambda_{\perp}(T)$ on the single domain states. The reference length is chosen just above T_N, at $T=21$ K. Although unspectacular, for a Tb based cubic compound, with a maximum amplitude of 1.5×10^{-4} at low temperature, the tetragonal symmetry lowering is very well characterized. Below T_N, the system elongates along its fourfold axis and contracts along a perpendicular direction. At T_N, the tetragonal strain cancels abruptly, which is an additional proof for the first-order character of the magnetic transition.

In the thermal dependence of the volume mode ϵ^{α}, after a peak that may be ascribed to domains rearrangement close to T_N, a negative discontinuity is also observed, with a small magnitude of about 3×10^{-6}. Such a negative thermal expansion at T_N, i.e., an antiferromagnetic state with larger volume than the paramagnetic one, has been also observed in GdB_6,[21] with similar amplitude. This similar effect in systems with and without $4f$ orbital degeneracy indicates that it doesn't derive from the crystal field, but most likely results from the volume dependence of the exchange energy. Indeed, due to the complex dependence of the RKKY coupling on the distance between the magnetic ions, a negative expansion is not unlikely. In all cases, this volume effect remains quite small in comparison to the tetragonal strain: this is a regular feature in rare-earth cubic intermetallics where the $4f$ quadrupoles, responsible for the main magnetostrictive effects, are not coupled with the volume, but with the symmetry lowering strain modes.[3]

B. X-ray diffraction investigation

The x-ray experiments were performed at the ESRF, on the ID10A beamline. A photons wavelength, $\lambda=0.6632$ Å, was selected from the (111) reflection on a diamond monochromator. The use of the diamond (111) reflection ensures

negligible higher harmonics contamination of the incident beam, which reduces the risk of confusion of displacement reflections with $\lambda/2$ lattice scattering. Short wavelengths are required in order to reach reflections with large Q, where larger scattering intensities are expected in case of diffraction by atomic displacements[5] or rare-earth multipoles waves.[22] Another advantage of high-energy photons is a larger penetration depth, thus a larger scattering volume with less surface related effects. One effect that can be thus mitigated is the reduction of the intensity of part of the reflections as result of the magnetoelastic segregation of domains by the surface. Such an effect is observed in NdMg,[22] a system also undergoing a tetragonal symmetry lowering below T_N. In addition, the high energy of the incident beam is far enough from the absorption edges of both Tb and B, which ensures minimal incoherent scattering contribution to the measured reflections. In order to obtain a small flat surface, perpendicular to the [001] axis, the TbB_6 sphere had been slightly altered by grinding. The sample was mounted inside the ID10A closed-cycle refrigerator, in such a way that, for zero tilting angle of the cryostat, the horizontal scattering plane was in coincidence with the sample's (100) plane. The goniometer being set for scattering inside the horizontal plane, specular reflections (i.e., Bragg reflections from crystal planes parallel to the sample surface) from the flat sample face of the (00l) type were accessible. At $T=7.5$ K, the base temperature of the closed-cycle refrigerator, an extended collection of ω scans was performed for $\boldsymbol{Q}$ vectors in relation with the expected wave vectors for charge phenomena (i.e., quadratically related to the magnetic structure of wave vectors $\langle\frac{1}{4}\frac{1}{4}\frac{1}{2}\rangle$): $\langle\frac{1}{2}00\rangle$, $\langle\frac{1}{2}\frac{1}{2}0\rangle$, $\langle\frac{1}{4}\frac{1}{4}\frac{1}{2}\rangle$, and $\langle\frac{1}{4}\frac{1}{4}0\rangle$.

In this collection, the only sizable intensities were obtained for Q vectors in relation with $\langle\frac{1}{2}00\rangle$ and $\langle\frac{1}{2}\frac{1}{2}0\rangle$ wave vectors. The intensities of the reflections were determined by integrating the rocking curve scans. Corrected from the Lorentz and polarization factors, they were normalized using 14 main Bragg reflections of the CaB_6 structure in order to obtain an experimental structure factor in equivalent Thomson electrons. Note that the experimental structure factors of the $\langle\frac{1}{2}\frac{1}{2}0\rangle$-type reflections are one order of magnitude smaller than those of the $\langle\frac{1}{2}00\rangle$-type, but are still larger than the maximum expected in case of Thomson multipolar scattering by the Tb^{3+} ions.[22,23] Nonetheless, as shown in Fig. 6, the normalized structure factors for the $(00\frac{13}{2})$ and $(0\frac{1}{2}\frac{13}{2})$ representative reflections have, within the error bars, an identical thermal dependence between 7.5 and 25 K. Both of the monitored reflections vanish abruptly at T_N, which confirms their link with the antiferromagnetic state and the first-order character of the magnetic transition.

The hypothesis of displacement waves resulting in the observed reflections can be tested via the Q dependence of the scattering factor. Figure 7 shows the experimental structure factor for all the specular $(00\frac{l}{2})$ reflections. Considering an antiphase displacement wave, with $\boldsymbol{q}$ wave vector and $\boldsymbol{\delta}_q$ Fourier component, neglecting all crystallographic effects except the displacement of the Tb^{3+} ion, the real structure factor for a scattering vector $\boldsymbol{Q}=\boldsymbol{H}\pm\boldsymbol{q}$ (where $\boldsymbol{H}$ belongs to the reciprocal lattice) reads as

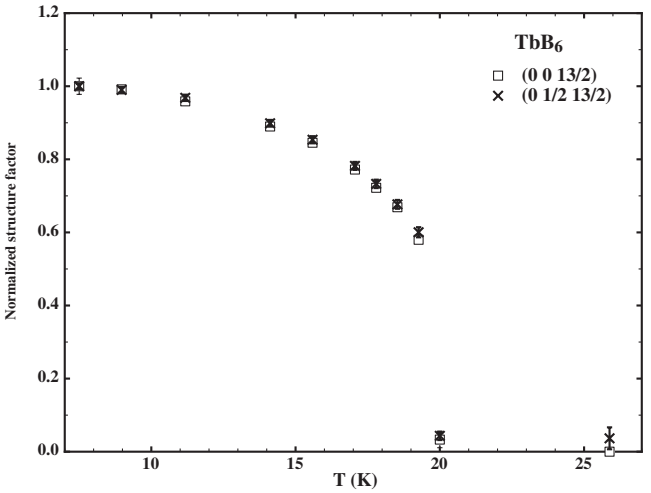

FIG. 6. Thermal variation of the normalized experimental structure factors for the $(00\frac{13}{2})$ and $(0\frac{1}{2}\frac{13}{2})$ reflections.

$$F(\boldsymbol{Q}) = f_{Tb}(Q)\sin(\boldsymbol{Q}\,.\,\boldsymbol{\delta}_q), \tag{4}$$

where $f_{Tb}(Q)$ is the Thomson scattering factor for Tb^{3+}. Exchange displacement waves propagated by $\langle 00\frac{1}{2}\rangle$ vectors are predicted to be longitudinal,[5] which means there are no alternatives for the $\boldsymbol{\delta}_q$ Fourier component direction. Considering that δ_q is small, in comparison with the lattice parameter, assuming domains equipartition and an equal amplitude for all the N_q Fourier components, the practical scattering factor reads as

$$F(\boldsymbol{Q}) = \sqrt{\frac{N_q}{3}} f_{Tb}(Q)(\boldsymbol{Q}\,.\,\boldsymbol{\delta}_q). \tag{5}$$

Using this formula, the Q dependence reported in Fig. 7 is fairly well reproduced for $\sqrt{N_q/3}(\delta_q/a)=2.6\times10^{-3}$, where a is TbB_6 lattice parameter. Considering the high symmetry,

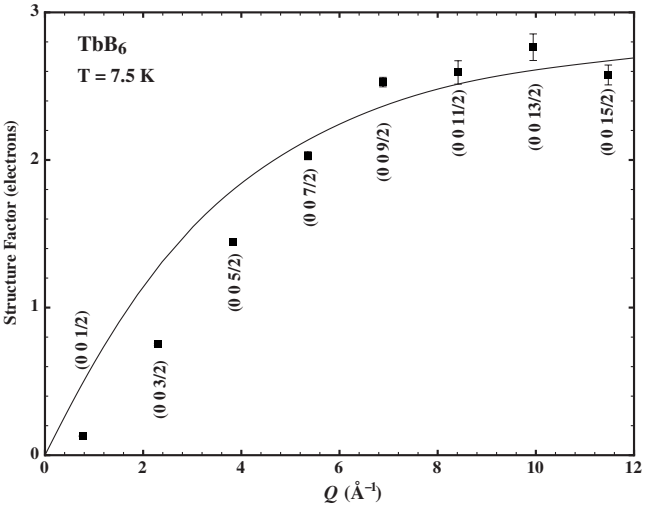

FIG. 7. Experimental structure factors (full diamonds) of the specular $\langle 00\frac{1}{2}\rangle$-type reflections at 7.5 K in TbB_6. The full line represents the calculated structure factor, which is proportional to the product $f_{Tb}(Q)Q$.

constant amplitude, single-q, double-q, and triple-q displacements models, this value yields a total relative displacement of Tb^{3+} ion: $\delta/a=4.5\times10^{-3}$ at $T=7.5$ K. This magnitude of the displacement compares well with the value, $\delta/a=3.9\times10^{-3}$, determined in the high-temperature phase of GdB_6.[5] The discrepancies observed at low $\boldsymbol{Q}$, which are reminiscent of the GdB_6 case, could results from the screening of the Tb^{3+} displacement by the conduction electrons. Except for this slight deviation at small angles, the Q dependence of the $(00\frac{l}{2})$ scattering factor appears consistent with the hypothesis of the displacement waves.

Unfortunately such a clear Q dependence could not be evidenced for the off-specular reflections of both the $\langle\frac{1}{2}00\rangle$ and $\langle\frac{1}{2}\frac{1}{2}0\rangle$ families. One observes quite a large dispersion of the experimental structure factors for equivalent reflections, even after correction of the absorption effects. At this point, in absence of reliable quantitative data the origin of the $\langle0\frac{1}{2}\frac{1}{2}\rangle$ reflections remains unclear.

III. ANTIFERROMAGNETIC MODELS FOR TbB_6

Here, our aim is not a computational description of TbB_6 order properties but rather to define its most probable magnetic structure from theoretical and experimental arguments. The models describing the ordering properties of rare-earth intermetallic compounds are usually based on a Hamiltonian including the exchange interactions and the crystal electric field term. In cubic compounds, additional interactions are often necessary, in particular the quadrupolar[3] ones. In the case of TbB_6, as for GdB_6, it appears that one essential ingredient is the exchange and elastic corrections introduced by the atomic displacements. Criteria reflecting the minimization the exchange and displacement energies should be effective in extracting, from a set of possible magnetic structures, the most probable one. The starting point is here to define these criteria thanks to a mean-field description of the exchange displacements. Using the experimental data to define the set of viable models, a few or even a single magnetic structure should emerge from this analysis.

A. Mean-field description of exchange displacements

The model describing the exchange induced atomic displacements was introduced in the paper devoted to the GdB_6 case.[5] It accounts for the RKKY interaction dependence on the distance between the rare-earth ions, which are supposed to sit in a harmonic well. In this context, for a large set of N interacting ions, the simplest corrective Hamiltonian term reads as

$$\mathcal{H}_d=-\sum_{i\neq j}[\boldsymbol{g}_{ij}\cdot(\boldsymbol{d}_j-\boldsymbol{d}_i)]\boldsymbol{J}_i\cdot\boldsymbol{J}_j+\sum_{i=1}^{N}A^{\alpha}\boldsymbol{d}_i^2. \tag{6}$$

In this expression, the individual displacements $\boldsymbol{d}$, with respect to the paramagnetic equilibrium position, are treated as parameters and the first sum is over all the (ij) pairs of ions of respective total momentum $\boldsymbol{J}_i$ and $\boldsymbol{J}_j$. The vector $\boldsymbol{g}_{ij}$ is the gradient, with respect to the position of ion j, i being fixed, of the isotropic exchange coupling constant $(\boldsymbol{g}_{ij}=-\boldsymbol{g}_{ji})$. The strength of the "restoring force" is described in the last term by the constant A^{α}.

In the mean-field approximation, for a given site i, the exchange-displacements corrective term is translated into a single-ion Hamiltonian as

$$\mathcal{H}_{d_i}=-d\boldsymbol{H}_i^m\boldsymbol{J}_i+A^{\alpha}\boldsymbol{d}_i^2, \tag{7}$$

where the mean-field correction identifies with

$$d\boldsymbol{H}_i^m=\sum_{j,j\neq i}[\boldsymbol{g}_{ij}\cdot(\boldsymbol{d}_j-\boldsymbol{d}_i)]\langle\boldsymbol{J}_j\rangle. \tag{8}$$

Minimizing the associated internal energy correction with respect to $\boldsymbol{d}_i$, one gets the displacement equilibrium value:

$$\boldsymbol{d}_i=-\frac{1}{2A^{\alpha}}\sum_{j,j\neq i}(\langle\boldsymbol{J}_j\rangle\cdot\langle\boldsymbol{J}_i\rangle)\boldsymbol{g}_{ij}. \tag{9}$$

According to this relation, a displacements scheme can be, in principle, derived for any magnetic structure. In doing this, the difficulty comes from the unknown $\boldsymbol{g}_{ij}$, but it can be solved or alleviated taking advantage of the system symmetries, both in direct and reciprocal spaces.

B. Use of Fourier analysis

1. Magnetic and displacive Fourier series

As the magnetic moments, the atomic displacements have well-defined periodicities revealed by x-ray diffraction. Fourier analysis can be thus used in the treatment of Eq. (7) mean-field Hamiltonian, replacing the magnetic moments and the displacements with their Fourier series expansions. The magnetic Fourier series defining the magnetic moment at site i, located at $\boldsymbol{R}_i$, consist of the components $\boldsymbol{m}_{\boldsymbol{k}}$ and wave vectors $\boldsymbol{k}$ defining the magnetic structure:

$$\boldsymbol{m}_i=\langle\boldsymbol{J}_i\rangle=\sum_{\boldsymbol{k}}\boldsymbol{m}_{\boldsymbol{k}}\exp[j\boldsymbol{k}\cdot\boldsymbol{R}_i], \tag{10}$$

where $j^2=-1$ and the sum is over all members of the magnetic wave-vector star. Then, introducing the vector $\boldsymbol{\Gamma}_{\boldsymbol{k}}$ defining the Fourier transform of the couplings gradient $\boldsymbol{g}_{ij}$:

$$\boldsymbol{\Gamma}_{\boldsymbol{k}}=\sum_{j,j\neq i}\boldsymbol{g}_{ij}\exp[-j\boldsymbol{k}\cdot(\boldsymbol{R}_j-\boldsymbol{R}_i)], \tag{11}$$

one may rewrite Eq. (9) as

$$\boldsymbol{d}_i=\frac{1}{2A^{\alpha}}\sum_{\boldsymbol{k},\boldsymbol{k}'}(\boldsymbol{m}_{\boldsymbol{k}}\cdot\boldsymbol{m}_{\boldsymbol{k}'})\boldsymbol{\Gamma}_{\boldsymbol{k}}\exp[j(\boldsymbol{k}+\boldsymbol{k}')\cdot\boldsymbol{R}_i], \tag{12}$$

which shows that the displacement wave vectors $\boldsymbol{q}$ are all of the form $\boldsymbol{q}=\boldsymbol{k}+\boldsymbol{k}'$ where $\boldsymbol{k}$ and $\boldsymbol{k}'$ are magnetic wave vectors. Moreover, the polarization of the displacement waves depends entirely on the $\boldsymbol{\Gamma}_k$ vectors, which directions can be specified from symmetry arguments only. In case of the magnetic wave vector star $\langle\frac{1}{4}\frac{1}{4}\frac{1}{2}\rangle$ and for the representative magnetic wave vector $[\frac{1}{4}\frac{1}{4}\frac{1}{2}]$, it can be shown[5] that: $\boldsymbol{\Gamma}_{[\frac{1}{4}\frac{1}{4}\frac{1}{2}]}=\pm j\frac{G}{\sqrt{2}}[110]$, where G is the amplitude of $\boldsymbol{\Gamma}_k$. The longitudinal character of the $\langle\frac{1}{2}00\rangle$ displacements waves results from this alignment of the $\boldsymbol{\Gamma}_k$ vectors along twofold axes.

2. Displacive correction of the periodic mean field

Introducing the magnetic and displacive Fourier series in the definition of the mean-field correction and using definition (11) of $\mathbf{\Gamma}_k$, Eq. (8) becomes

$$d\boldsymbol{H}_i^m = \frac{1}{2A^\alpha} \sum_{\boldsymbol{k},\boldsymbol{k}',\boldsymbol{k}''} [\mathbf{\Gamma}_{\boldsymbol{k}''} \cdot (\mathbf{\Gamma}_{\boldsymbol{k}} - \mathbf{\Gamma}_{\boldsymbol{k}+\boldsymbol{k}'+\boldsymbol{k}''})] \times (\boldsymbol{m}_{\boldsymbol{k}'} \cdot \boldsymbol{m}_{\boldsymbol{k}''})\boldsymbol{m}_{\boldsymbol{k}} \exp[j(\boldsymbol{k}+\boldsymbol{k}'+\boldsymbol{k}'') \cdot \boldsymbol{R}_i], \quad (13)$$

where each sum is over all members of the magnetic wave vector star. To ensure the stability of the magnetic structure, the mean-field correction in Eq. (13) has to display the same periodicities as the magnetic moments. It is then necessary (but not sufficient) that the wave vectors resulting from the sum $\boldsymbol{k}+\boldsymbol{k}'+\boldsymbol{k}''$ belong to the set of wave vectors describing the magnetic structure. The minimal set of wave vectors for describing a real magnetic structure is $A=\{\boldsymbol{k},-\boldsymbol{k}\}$ which implies that the vectors $\boldsymbol{k}+\boldsymbol{k}'+\boldsymbol{k}''$ belong to the set: $B=\{\boldsymbol{k}, -\boldsymbol{k}, 3\boldsymbol{k}, -3\boldsymbol{k}\}$. A and B need to be identical which requires the equivalencies: $3\boldsymbol{k} \equiv \boldsymbol{k}$ or $3\boldsymbol{k} \equiv -\boldsymbol{k}$. This, respectively, translates into the equations:

$$2\boldsymbol{k} = \boldsymbol{H} \text{ or } 4\boldsymbol{k} = \boldsymbol{H},$$

where $\boldsymbol{H}$ is a node of the paramagnetic reciprocal lattice. Within the first Brillouin zone, the first equation is consistent with magnetic wave vectors belonging to the $\langle \frac{1}{2}\frac{1}{2}\frac{1}{2}\rangle$, $\langle \frac{1}{2}\frac{1}{2}0\rangle$, and $\langle \frac{1}{2}00\rangle$ stars. Magnetic structures based on such wave vectors are centrosymmetric and cannot result in the formation of displacement waves. Displacement waves and the associated exchange correction can only emerge for wave vectors obeying the equation $\boldsymbol{k}=\boldsymbol{H}/4$, i.e., in the first Brillouin zone: $\langle \frac{1}{4}\frac{1}{4}\frac{1}{4}\rangle$, $\langle \frac{1}{4}\frac{1}{4}\frac{1}{2}\rangle$, $\langle \frac{1}{4}\frac{1}{4}0\rangle$, $\langle \frac{1}{4}\frac{1}{2}\frac{1}{2}\rangle$, $\langle \frac{1}{4}\frac{1}{2}0\rangle$, and $\langle \frac{1}{4}00\rangle$.

If one considers the antiferromagnetic elements in R-B_6 series, a striking data is the recurrence[10,24–26] of one of the above listed wave vector stars: $\langle \frac{1}{4}\frac{1}{4}\frac{1}{2}\rangle$. The only exception is NdB_6 which orders in a simple $\langle \frac{1}{2}00\rangle$ collinear structure.[27] It is unlikely that, for most elements in this series, the maximum of the exchange coupling coincides with $\langle \frac{1}{4}\frac{1}{4}\frac{1}{2}\rangle$. This particular wave vector is selected because, with help of the atomic displacements, a lower antiferromagnetic free energy is achieved. In the R-B_6 series, the atomic displacements waves are then active in the locking of the magnetic wave vector at the commensurate $\langle \frac{1}{4}\frac{1}{4}\frac{1}{2}\rangle$.

The energy gain results from a reinforced mean field as described by Eq. (13). The implications of this correction can be more easily analyzed in the context of a minimalist antiferromagnetic structure $\{(\boldsymbol{k},\boldsymbol{m}_{\boldsymbol{k}}),(-\boldsymbol{k},\boldsymbol{m}_{-\boldsymbol{k}})\}$. In absence of atomic displacements, for an antiferromagnet with wave vectors belonging to a unique star $\langle \boldsymbol{k} \rangle$, the isotropic exchange mean field acting at site i can be factorized into the form:

$$\boldsymbol{H}_i^{m0} = J^0(\boldsymbol{k})\boldsymbol{m}_i, \quad (14)$$

where $J^0(\boldsymbol{k})$ is the Fourier transform of the exchange coupling for a representative magnetic wave vector $\boldsymbol{k}$. Equation (14) shows that, in the mean-field description of isotropic exchange, a unique site is representative of the whole system. Consequently, all the magnetic sites have in common the amplitudes of their mean field and magnetic moment. A favorable displacement scheme should uniformly reinforce the mean field, which implies a corrective mean field in the same form as Eq. (14). Expanding Eq. (13) for the elementary antiferromagnetic structure, with a wave vector such that $\boldsymbol{k}=\boldsymbol{H}/4$, the mean-field correction can be brought to the form

$$d\boldsymbol{H}_i^m = \frac{G^2}{A^\alpha} m^2 \boldsymbol{m}_i, \quad (15)$$

where m is the constant amplitude of the magnetic moment. This form requires the real and imaginary parts of $\boldsymbol{m}_{\boldsymbol{k}}$ (respectively, $\boldsymbol{m}_{-\boldsymbol{k}}$) to be parallel and of equal amplitudes. Within these conditions, the elementary magnetic structure is necessarily collinear (i.e., an helical configuration is ruled out) and the mean field is uniformly reinforced. This reinforcement can be strong enough to determine a first-order magnetic transition at T_N, as observed in the GdB_6 case.[5]

C. Antiferromagnetic models

The macroscopic experimental data point to a model with a tetragonal symmetry. More precisely, from magnetic susceptibility and magnetostriction measurements (Secs. II A 1 and II A 2), one can infer that a multiaxial magnetic arrangement is stabilized in the plane perpendicular to the fourfold axis of the tetragonal structure. Moreover, as the antiferromagnetic state of TbB_6 involves a single magnetic wave-vector star and is stable down to the minimum temperature, the magnetic moments amplitude should be the same on all sites.

From the powder neutron-diffraction patterns, it was deduced that the Fourier component propagated by $[\frac{1}{4}\frac{1}{4}\frac{1}{2}]$ is along the [001] direction.[10] The possible directions for the magnetic Fourier components are then the three fourfold axes of the cubic system. To build a planar, multiaxial structure, one has to associate two of these directions. In case of equal amplitude for the two respective components, the total magnetic moment lies along a twofold axis. This is not in conflict with the crystal-field anisotropy expected for an initially cubic system: twofold axes are among the possible favored directions, provided the transition at T_N is first-order, which is precisely the case in TbB_6. At this point, the required characteristics of the magnetic structure of TbB_6 are: tetragonal, multiaxial, and planar (in the plane perpendicular to the fourfold axis) with magnetic moments along twofold axes.

In addition, using the exchange displacements model, one can check the consistency of any candidate magnetic structure with the observed x-ray satellites. This same model also provides physical criteria which are helpful for defining realistic magnetic structures.

In order to build the magnetic models, the fourfold axis is here arbitrarily chosen along the [001] direction. Then, the two components, which result in a total magnetic moment along twofold axes, are parallel to the [100] and [010] directions. In a first step, it is convenient to treat them separately and the discussion is here focused on the magnetic component parallel to [100]. For this particular direction, the possibly involved wave vectors belong to the set:$\{[\frac{1}{2}\frac{1}{4}\frac{1}{4}],[\frac{1}{2}\frac{\bar{1}}{4}\frac{\bar{1}}{4}],[\frac{1}{2}\frac{\bar{1}}{4}\frac{1}{4}],[\frac{1}{2}\frac{1}{4}\frac{\bar{1}}{4}]\}$. Another simplification is

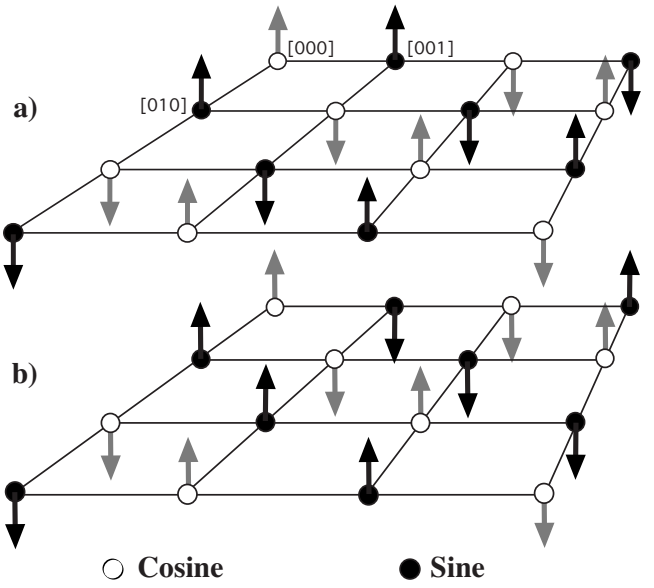

FIG. 8. Planar representations for the two kinds of magnetic fourfold components which serve as basis for TbB_6 multiaxial magnetic models. (a) Sine and cosine components sharing the same $[\frac{1}{2}\frac{1}{4}\frac{1}{4}]$ wave vector. (b) Sine and cosine components with, respectively, $[\frac{1}{2}\frac{1}{4}\frac{1}{4}]$ and $[\frac{1}{2}\frac{\bar{1}}{4}\frac{1}{4}]$ wave vectors. Open and full circles distinguish between the nonzero cosine or sine sites.

achieved if one considers this partial, collinear, structure in terms of its real (cosine) and imaginary (sine) components. Then, the above set of wave vectors reduces to $\{[\frac{1}{2}\frac{1}{4}\frac{1}{4}],[\frac{1}{2}\frac{\bar{1}}{4}\frac{1}{4}]\}$ and, in any Tb plane parallel to (100), the sine and cosine waves cancel at alternate sites. In such a plane, the sites with nonzero cosine, respectively, sine, component are organized in a square lattice (see Fig. 8, where the open and full circles refer to the sites of nonzero cosine, respectively, sine, components). To ensure a constant amplitude of the magnetic moment for both the sine and cosine lattices, a single sine, respectively, cosine, component must be active. Building the partial collinear structure with moments along [100] then consists in selecting two components, one for each, sine and cosine, network. These two components may share or not the same wave vector which, in fine, defines only two solutions, *a* and *b*, represented on Fig. 8 (symmetry equivalent solutions may be obtained, for instance, via a shift of the origin, or, for *a*, via a $\frac{\pi}{2}$ rotation about the [100] direction).

In Table III the magnetic Fourier components of models *a* and *b* are listed, as well as their displacements counterparts derived from Eq. (12). Models a' and b' are the corresponding solutions, obtained via a $\pi/2$ rotation about [001], for a magnetic component along [010]. From Eq. (13), one can check that all the collinear magnetic models of Table III result in the same mean-field correction of Eq. (15). Type *a* and *b* are thus degenerate solutions in terms of exchange-displacements corrections.

Finally, the total magnetic model is built by associating two of these collinear solutions, one for each of the magnetic components directions: [100] and [010]. Although solutions *a* and *b* are, separately, consistent models with respect to the mean-field correction, the multiaxial association does not need to. Cross-terms can emerge in the sum of Eq. (13) and may destabilize the magnetic structure. This will occur in case the additional terms do not equally reinforce all of the Fourier components or if they introduce extra wave vectors in the mean-field correction. Therefore, for each multiaxial model, one has to define the cross-terms in Eq. (13) in order to check its stability under the effect of the mean-field correction. Subsequently, if more than one model is found stable, they can be compared to identify the one with the most favorable mean-field correction (i.e., with the lowest energy when considering the exchange displacement phenomenon).

1. Tetragonal models

According to the macroscopic measurements, TbB_6 antiferromagnetic state shows a tetragonal symmetry. To respect this requirement, a model with a fourfold axis along the *z* direction [001] can be built by associating two collinear solutions of the same kind, one transforming into the other through a $\pm\pi/2$ rotation about [001] (plus a possible translation that has no consequence at the macroscopic level). Starting with the components of models *a* and *b* in Table III,

TABLE III. Wave vectors $(\boldsymbol{k},\boldsymbol{q})$ and Fourier components $(\boldsymbol{m}_{\boldsymbol{k}},\boldsymbol{d}_{\boldsymbol{q}})$ describing the magnetic (upper rows) and displacements (lower rows) parts of the partial, fourfold models *a*, a', *b*, and b'. Models a' and b' are, respectively, derived from *a* and *b* through a rotation of $+\pi/2$ about the [0 0 1] axis. *m* is the amplitude of the magnetic moment. The magnetic Fourier components are given here in terms of cosine $(\boldsymbol{m}_{\boldsymbol{k}}^{\boldsymbol{c}})$ and sine $(\boldsymbol{m}_{\boldsymbol{k}}^{\boldsymbol{s}})$ components. This set of models is not exhaustive as there exist symmetry equivalents. It is, however, representative, starting from an arbitrary choice of the first (left) cosine magnetic component. There are subsequent $\pm$ alternatives for the associated sine component as well as for the deduced displacements.

a			a'			*b*			b'		
$\boldsymbol{k}$	$\boldsymbol{m}_{\boldsymbol{k}}^{\boldsymbol{c}}$	$\boldsymbol{m}_{\boldsymbol{k}}^{\boldsymbol{s}}$	$\boldsymbol{k}$	$\boldsymbol{m}_{\boldsymbol{k}}^{\boldsymbol{c}}$	$\boldsymbol{m}_{\boldsymbol{k}}^{\boldsymbol{s}}$	$\boldsymbol{k}$	$\boldsymbol{m}_{\boldsymbol{k}}^{\boldsymbol{c}}$	$\boldsymbol{m}_{\boldsymbol{k}}^{\boldsymbol{s}}$	$\boldsymbol{k}$	$\boldsymbol{m}_{\boldsymbol{k}}^{\boldsymbol{c}}$	$\boldsymbol{m}_{\boldsymbol{k}}^{\boldsymbol{s}}$
$[\frac{1}{2}\frac{1}{4}\frac{1}{4}]$	$[m00]$	$\mp[m00]$	$[\frac{\bar{1}}{4}\frac{1}{2}\frac{1}{4}]$	$[0m0]$	$\mp[0m0]$	$[\frac{1}{2}\frac{1}{4}\frac{1}{4}]$	$[m00]$		$[\frac{\bar{1}}{4}\frac{1}{2}\frac{1}{4}]$	$[0m0]$	
$[\frac{1}{2}\frac{\bar{1}}{4}\frac{1}{4}]$			$[\frac{1}{4}\frac{1}{2}\frac{1}{4}]$			$[\frac{1}{2}\frac{\bar{1}}{4}\frac{1}{4}]$		$\mp[m00]$	$[\frac{1}{4}\frac{1}{2}\frac{1}{4}]$		$\mp[0m0]$
$\boldsymbol{q}$	$\boldsymbol{d}_{\boldsymbol{q}}$		$\boldsymbol{q}$	$\boldsymbol{d}_{\boldsymbol{q}}$		$\boldsymbol{q}$	$\boldsymbol{d}_{\boldsymbol{q}}$		$\boldsymbol{q}$	$\boldsymbol{d}_{\boldsymbol{q}}$	
$[0\frac{1}{2}\frac{1}{2}]$	$\pm\frac{G^2}{2\sqrt{2}A^a}m^2[011]$		$[\frac{1}{2}0\frac{1}{2}]$	$\pm\frac{G^2}{2\sqrt{2}A^a}m^2[\bar{1}01]$		$[0\frac{1}{2}0]$	$\pm\frac{G^2}{2\sqrt{2}A^a}m^2[0\bar{1}0]$		$[\frac{1}{2}00]$	$\pm\frac{G^2}{2\sqrt{2}A^a}m^2[100]$	
						$[00\frac{1}{2}]$	$\pm\frac{G^2}{2\sqrt{2}A^a}m^2[001]$		$[00\frac{1}{2}]$	$\pm\frac{G^2}{2\sqrt{2}A^a}m^2[001]$	

TABLE IV. Fourier description of the stable tetragonal models, $b_+\otimes b'_+$ and $b_+\otimes b'_-$, obtained by associating two fourfold models from Table III. Below the displacements Fourier components $(\boldsymbol{q},\boldsymbol{d}_q)$, the last row gives the mean-field correction at site i.

	$b_+\otimes b'_+$		$b_+\otimes b'_-$	
$\boldsymbol{k}$	$\boldsymbol{m}^c_k$	$\boldsymbol{m}^s_k$	$\boldsymbol{m}^c_k$	$\boldsymbol{m}^s_k$
$[\frac{1}{2}\frac{1}{4}\frac{1}{4}]$	$[\frac{m}{\sqrt{2}}00]$		$[\frac{m}{\sqrt{2}}00]$	
$[\frac{1}{2}\frac{\bar{1}}{4}\frac{1}{4}]$		$-[\frac{m}{\sqrt{2}}00]$		$-[\frac{m}{\sqrt{2}}00]$
$[\frac{\bar{1}}{4}\frac{1}{2}\frac{1}{4}]$	$[0\frac{m}{\sqrt{2}}0]$		$[0\frac{m}{\sqrt{2}}0]$	
$[\frac{1}{4}\frac{1}{2}\frac{1}{4}]$		$-[0\frac{m}{\sqrt{2}}0]$		$[0\frac{m}{\sqrt{2}}0]$
$\boldsymbol{q}$	$\boldsymbol{d}_q$		$\boldsymbol{d}_q$	
$[\frac{1}{2}00]$	$\frac{G^2}{4\sqrt{2}A^\alpha}m^2[100]$		$-\frac{G^2}{4\sqrt{2}A^\alpha}m^2[100]$	
$[0\frac{1}{2}0]$	$-\frac{G^2}{4\sqrt{2}A^\alpha}m^2[010]$		$-\frac{G^2}{4\sqrt{2}A^\alpha}m^2[010]$	
$[00\frac{1}{2}]$	$\frac{G^2}{2\sqrt{2}A^\alpha}m^2[001]$		0	
$d\boldsymbol{H}^m_i$	$\frac{3}{4}\frac{G^2}{A^\alpha}m^2\boldsymbol{m}_i$		$\frac{1}{4}\frac{G^2}{A^\alpha}m^2\boldsymbol{m}_i$	

one first derives their rotated equivalents a' and b', before combining them. The tetragonal model thus obtained must be stable with respect to its mean-field correction, which is checked using Eq. (13).

All models based on (aa') associations appear to be unstable with respect to their mean-field correction: from the cross-terms in Eq. (13), additional mean-field exchange terms emerge with $\langle\frac{1}{4}\frac{1}{4}0\rangle$ wave vectors. The only associations which resist the stability test are of the form (bb'), which, including a $(\pm)$ alternative, consists in two models. These tetragonal stable models are described in Table IV. In the last row, the mean-field correction for these models show they bring less benefit, as regards the exchange and displacement energy, than the basic collinear models of Table III. Obviously, to explain the stabilization of a multiaxial magnetic structure, one should also consider pair interactions beyond the isotropic exchange, the most commonly invoked ones being the quadrupolar couplings.[3] With respect to the exchange displacements correction, the most favorable multiaxial mode, $b_+\otimes b'_+$, is represented on Fig. 9. It corresponds to the maximum amplitude for the Tb displacements, which are directed along $\langle 112\rangle$ axes. As the displacement elastic energy is here restricted to a quadratic term [see Eq. (6)], it is isotropic and displacements along such a low-symmetry direction cannot be ruled out. Accounting for the displacement anisotropy could favor the alternative tetragonal model $b_+\otimes b'_-$, which, although penalized by its reduced mean-field correction, results in displacements along the higher symmetry $\langle 110\rangle$ axes.

From the displacements point of view, the two stable tetragonal models are associated with multi-q $\langle\frac{1}{2}00\rangle$ structures. Such wave vectors are indeed observed in the x-ray diffraction experiments. However, their are not exclusive since less intense satellites, related to the $\langle\frac{1}{2}\frac{1}{2}0\rangle$ wave vectors, are as well detected. One could ascribe them, as in the case of GdB_6 high-temperature phase, to a second-order scattering phenomena arising from the multi-q $\langle\frac{1}{2}00\rangle$ displacements. However, the second-order scattering amplitude being quadratically related to the first-order one, this hypothesis is in contradiction with the parallel thermal dependences of the two kind of satellites (Fig. 6).

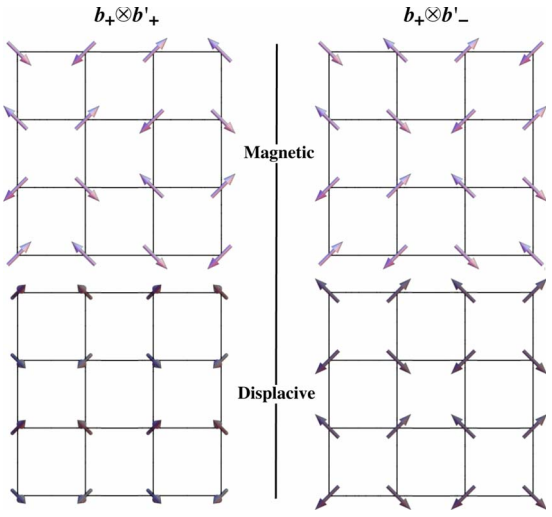

FIG. 9. (Color online) Magnetic (upper part) and displacive (lower part) arrangements which correspond to the stable tetragonal models for TbB_6 antiferromagnetic state. Models $b_+\otimes b'_+$ and $b_+\otimes b'_-$ in Table IV. In model $b_+\otimes b'_+$, the magnetic planes are stacked in a $(++--)$ sequence along the perpendicular fourfold axis, whereas in $b_+\otimes b'_-$ the moments from two successive planes are rotated through a $\pi/2$ angle. The $b_+\otimes b'_+$ displacement vectors are out of plane and directed along $\langle 112\rangle$ directions.

An alternative explanation for the extra x-ray reflections could be multipolar $4f$ scattering, the first relevant order being the quadrupolar one. The quadrupolar arrangements consistent with the magnetic structure can be derived in the assumption that the quadrupoles develop under the action of the exchange mean field (see Ref. 28, for instance). Considering the above tetragonal models, with magnetic moments along twofold axes perpendicular to the fourfold, z axis, the only ordered quadrupolar components are O^0_2 and P_{xy}. Their relations to the exchange mean field, thus to the magnetic components at site i read as $\langle O^0_2\rangle_i = C_\gamma(3m_{zi}-m_i^2)$ and $\langle P_{xy}\rangle_i = C_\epsilon m_{xi}m_{yi}$. Where the C_γ and C_ϵ constants are, at a given temperature, common to all sites. As there is no magnetic component along the z axis, $\langle O^0_2\rangle$ is constant from site to site, i.e., it represents a ferroquadrupolar component which, via the magnetoelastic coupling,[3] is the main contributor to the observed magnetostriction phenomenon. From Table IV, the products resulting in the $\langle P_{xy}\rangle$ quadrupolar components can only yield wave vectors in the $\langle\frac{1}{4}\frac{1}{4}0\rangle$ star for $b_+\otimes b'_+$ and in the $\langle\frac{1}{4}\frac{1}{4}\frac{1}{2}\rangle$ star for $b_+\otimes b'_-$. Therefore, for the considered tetragonal models, quadrupolar x-ray scattering cannot be responsible for the observed $\langle\frac{1}{2}\frac{1}{2}0\rangle$ reflections.

2. Lower symmetry models

From Eq. (12), it is clear that perpendicular magnetic Fourier components cannot bring a specific contribution to the atomic displacements. Therefore, associating two perpendicular models from Table III), in order to build a multiaxial magnetic structure, does not result in new displacements

Fourier components. The only possible displacements wave vectors are those already present in the two collinear models. Now, if one ascribes both the $\langle \frac{1}{2}00 \rangle$ and $\langle \frac{1}{2}\frac{1}{2}0 \rangle$ charge satellites to atomic displacements waves, a multiaxial magnetic structure can be proposed which combines a type *a* collinear model, which yields the $\langle \frac{1}{2}\frac{1}{2}0 \rangle$ wave vectors, with a perpendicular type *b*, which results in $\langle \frac{1}{2}00 \rangle$ displacements. Obviously, since the perpendicular magnetic contributions are not related by a $\pi/2$ rotation, the resulting magnetic structure cannot be of tetragonal symmetry. However, if the two magnetic contributions are of close enough amplitude, from macroscopic investigation techniques the resulting multiaxial structure might be confused with a tetragonal one.

Unfortunately, all such low-symmetry associations fail the stability test based on Eq. (13): additional exchange mean-field terms appear for $\langle \frac{1}{4}\frac{1}{4}0 \rangle$ wave vectors, as well as for initially inactive $\langle \frac{1}{4}\frac{1}{4}\frac{1}{2} \rangle$ nodes. The effective model, that could be iteratively derived from such combinations, would be then of a very low symmetry. This can be already expected by considering the combined displacements, with $\langle \frac{1}{2}\frac{1}{2}0 \rangle$ and $\langle \frac{1}{2}00 \rangle$ wave vectors, which cannot result in an equal displacement amplitude on all sites. At this point, it is extremely difficult to imagine an interplay of interactions which could stabilize such a low-symmetry arrangement other the whole antiferromagnetic range of TbB_6. As regard the quadrupolar counterpart of these low-symmetry structures, in addition to the ferroquadrupolar $\langle O_2^0 \rangle$ component, at order 0, the $\langle P_{xy} \rangle$ components develop according to a mixture of $\langle \frac{1}{4}\frac{1}{4}0 \rangle$ and $\langle \frac{1}{4}\frac{1}{4}\frac{1}{2} \rangle$ wave vectors. As for the tetragonal models, quadrupolar scattering cannot contribute to the $\langle \frac{1}{2}\frac{1}{2}0 \rangle$ charge reflections.

IV. CONCLUSIONS

From the magnetic-susceptibility investigation, the observed anisotropy in the antiferromagnetic phase of TbB_6 is characteristic of a tetragonal symmetry. This susceptibility is found maximum along the fourfold axis, which is evidence of the multiaxial character of the magnetic structure. This determination of the antiferromagnetic susceptibility anisotropy is essential for any subsequent experimental determination in the antiferromagnetic range. Indeed, applying a magnetic field along well chosen directions of the single crystal completely removes the domains distribution ambiguity. The investigation of TbB_6 antiferromagnetic magnetostriction illustrates the effectiveness of the field selection of domains: large steps in the sample length are observed as the sample switches from a single domain state to another. In the case of the used TbB_6 single crystal, once established, the single domain state is stable down to zero field. In these conditions, the spontaneous magnetostriction has been determined with unprecedented accuracy. All the observed magnetostriction behaviors are consistent with the symmetry conclusions derived from the magnetic susceptibility analysis: from all macroscopic aspects, the symmetry of TbB_6 antiferromagnetic state is tetragonal.

Below T_N, the x-ray diffraction experiments show rather intense $\langle \frac{1}{2}00 \rangle$-type reflections with a Q dependence characteristic of displacement waves. The GdB_6 case is then not singular among rare-earth hexaborides. In both compounds, the phenomena are of comparable amplitude, with a relative displacement of the rare-earth in the 10^{-3} range, and can account for the first-order transition at T_N. One of the proposed displacements scheme for TbB_6, biaxial with two $\langle \frac{1}{2}00 \rangle$ wave vectors, is identical to the one retained for GdB_6 high-temperature AF phase. However, the two magnetic structures differ, as GdB_6 is collinear, whereas TbB_6 is clearly multiaxial also on the magnetic side. This multiaxial character of TbB_6 magnetic structure cannot be accounted for considering the exchange displacements model, but could result from quadrupolar pair couplings which are absent in the $L=0$ gadolinium case. Other less intense charge reflections are also observed in TbB_6 AF state, in relation with $\langle \frac{1}{2}\frac{1}{2}0 \rangle$ wave vectors. Unfortunately, because of the experiment's geometry, the origin of these reflections couldn't be identified.

From a theoretical point of view, the observation of displacement waves in TbB_6 antiferromagnetic state gives a second opportunity to test and improve the exchange displacements model. Within the mean-field approximation, this model shows that the recurrence of the $\langle \frac{1}{4}\frac{1}{4}\frac{1}{2} \rangle$ magnetic wave vectors in the R-B_6 series is not fortuitous. This particular wave vector is among the few which can decrease the AF-state energy via the exchange displacement mechanism. As such, its recurrence in the rare-earth hexaborides series is the signature of the systematic development of exchange displacements waves.

Searching for tetragonal models consistent with the powder neutron diffraction, the macroscopic measurements and the exchange displacements stability criteria results in only two multiaxial solutions. These two models are associated with the formation of $\langle \frac{1}{2}00 \rangle$ displacements waves and are thus consistent with the main x-ray extra-reflections. However, they cannot account for the observation of the weaker $\langle \frac{1}{2}\frac{1}{2}0 \rangle$ reflections, except as result of second-order scattering by the multi-q displacement waves. This second order hypothesis is difficult to conciliate with the parallel thermal dependence of the two kinds of reflections. An alternative explanation, involving the scattering by $4f$ multipoles, cannot be retained: these reflections are too intense to be ascribed to off-resonant multipolar scattering and, moreover, the quadrupolar wave vectors deduced from the magnetic multiaxial models are not of the $\langle \frac{1}{2}\frac{1}{2}0 \rangle$ type. Further x-ray investigations are thus needed to clarify the origin of the $\langle \frac{1}{2}\frac{1}{2}0 \rangle$ reflections in TbB_6.

ACKNOWLEDGMENTS

The authors are particularly indebted to S. Kunii who provided the used single crystal, to F. Zontone for help on the ID10 beamline, and to D. Dufeu who developed the magnetostriction setup.

*Corresponding author. mehdi.amara@grenoble.cnrs.fr

[1] M. Ruderman and C. Kittel, Phys. Rev. **96**, 99 (1954).
[2] D. Gignoux and D. Schmitt, *Magnetism of Compounds of Rare Earths with Nonmagnetic Metals*, Handbook of Magnetic Materials Vol. 10 (Elsevier, Amsterdam, 1997), pp. 239–413, Chap. 2.
[3] P. Morin and D. Schmitt, *Quadrupolar Interactions and Magnetoelastic Effects in Rare Earth Intermetallic Compounds*, Ferromagnetic Materials (Elsevier Science, New York, 1990), pp. 1–132, Chap. 1.
[4] T. Kasuya, J. Magn. Magn. Mater. **174**, L28 (1997).
[5] M. Amara, S. E. Luca, R.-M. Galéra, F. Givord, C. Detlefs, and S. Kunii, Phys. Rev. B **72**, 064447 (2005).
[6] R. M. Galera, D. P. Osterman, and J. D. Axe, S. Kunii, and T. Kasuya,J. Appl. Phys. **63**, 3580 (1988).
[7] K. Segawa, A. Tomita, K. Iwashita, M. Kasaya, T. Suzuki, and S. Kunii, J. Magn. Magn. Mater. **104-107**, 1233 (1992).
[8] S. Granovsky, M. Amara, R.-M. Galéra, and S. Kunii, J. Phys.: Condens. Matter **13**, 6307 (2001).
[9] S. Nakamura, T. Goto, S. Kunii, K. Iwashita, and A. Tamaki, J. Phys. Soc. Jpn. **63**, 623 (1994).
[10] S. E. Luca, M. Amara, R. M. Galéra, F. Givord, S. Granovsky, O. Isnard, and B. Beneu, Physica B **350**, E39 (2004).
[11] S. Nakamura, T. Goto, A. Tamaki, S. Kunii, K. Iwashita, and M. Kasaya, Physica B **186-188**, 627 (1993).
[12] K. Takahashi and S. Kunii, J. Solid State Chem. **133**, 198 (1997).
[13] M. Wintenberger and R. Chamard-Bois, Acta Crystallogr., Sect. A: Cryst. Phys., Diffr., Theor. Gen. Crystallogr. **28**, 341 (1972).
[14] R. Aléonard, P. Morin, and J. Rouchy, J. Magn. Magn. Mater. **46**, 233 (1984).
[15] P. Morin, M. Giraud, P. Burlet, and A. Czopnik, J. Magn. Magn. Mater. **68**, 107 (1987).
[16] P. Morin and J. Pierre, Phys. Status Solidi (a) **30**, 549 (1975).
[17] L. Néel, J. Phys. Radium **5**, 241 (1944).
[18] A. Arrott, Phys. Rev. **108**, 1394 (1957).
[19] E. R. Callen and H. B. Callen, Phys. Rev. **129**, 578 (1963).
[20] M. Amara, I. Aviani, S. Luca, D. Dufeu, Ph. Lethuillier, and R. M. Galéra, J. Magn. Magn. Mater. **226-230**, 1005 (2001).
[21] S. Luca, Ph.D. thesis, Université Joseph-Fourier, Grenoble, 2002.
[22] M. Amara, R.-M. Galéra, P. Morin, and J.-F. Bérar, J. Phys.: Condens. Matter **10**, L743 (1998).
[23] M. Amara and P. Morin, J. Phys.: Condens. Matter **10**, 9875 (1998).
[24] J. Effantin, J. Rossat-Mignod, P. Burlet, H. Bartholin, and T. K. S. Kunii, J. Magn. Magn. Mater. **47-48**, 145 (1985).
[25] C. M. McCarthy, C. W. Tompson, R. J. Graves, H. W. White, Z. Fisk, and H. R. Ott, Solid State Commun. **36**, 861 (1980).
[26] K. Takahashi, H. Nojiri, K. Ohoyama, M. Ohashi, Y. Yamaguchi, M. Motokawa, and S. Kunii, J. Magn. Magn. Mater. **177-181**, 1097 (1998); International Conference on Magnetism (unpublished), Part Two
[27] C. M. McCarthy and C. W. Tompson, J. Phys. Chem. Solids **41**, 1319 (1980).
[28] M. Amara and P. Morin, Physica B **205**, 379 (1995).
[29] E. du Tremolet de Lacheisserie, D. Gignoux, and M. Schlenker, *Magnetism: Fundamentals* (Springer, Berlin, 2005), pp. 180–181.